Journal of Zhejiang University-SCIENCE A (Applied Physics & Engineering)
ISSN 1673-565X (Print); ISSN 1862-1775 (Online)
www.jzus.zju.edu.cn; www.springerlink.com
E-mail: jzus@zju.edu.cn

Hypoplastic modeling of soil-structure interfaces in offshore applications

Hans Henning STUTZ[†1], Frank WUTTKE[2]

[1]*Department of Engineering, Aarhus University, Aarhus 8000, Denmark*

[2]*Institute of Geo-Science, Kiel University, Kiel 24118, Germany*

[†]E-mail: hhs@eng.au.dk

Received Sept. 4, 2017; Revision accepted Feb. 23, 2018; Crosschecked July 9, 2018

Abstract: Cyclic and monotonic loaded offshore structures (e.g. piles, pipelines, cables, and suction-buckets) must be designed and calculated considering the effects of the soil-structure interaction. An advanced constitutive soil model must be used, but a simplified Mohr-Coulomb friction law is applied for the soil-structure interface. The Mohr-Coulomb model is a simple bilinear friction model that cannot take into account monotonic and cyclic interface phenomena. These include hardening, softening, and stiffness degradation under loading. However, we propose two advanced hypoplastic interface models for fine- and coarse-grained soils with intergranular strain concept. The intergranular strain concept has been proven to be an efficient way to model the small-strain deformation and un/reloading behavior of soils. The intergranular strain concept is therefore used to enhance the prediction capabilities of the hypoplastic interface models. Differences of the recent model formulation compared with previous versions are presented and discussed based on simulation. This is followed by an application of different models in finite-element simulations. The new models are used to simulate cyclic direct shear interface tests. Furthermore, the advanced interface model is used for simulation of a torodial penetrometer penetration problem. Several aspects, which are particularly important for offshore structures, are compared with the simple Mohr-Coulomb friction model.

Key words: Hypoplasticity; Interfaces; Cyclic loading; Fine and coarse grained soils
https://doi.org/10.1631/jzus.A1700469 **CLC number:** TU4

1 Introduction

The interface behavior of cyclic and monotonic loaded offshore structures (e.g. piles, anchors, and pipelines) is important for the service and limit state of the geotechnical structure. In the last three decades, many studies have highlighted the importance of soil-structure interfaces for global structural performance. Especially for cyclic loading paths, the interface should be considered accurately (DeJong et al., 2006; Mortara et al., 2007; DeJong and Westgate, 2009; Pra-ai and Boulon, 2017).

In addition to experimental evidence, different constitutive frameworks have been used to model the cyclic behavior of interfaces. Many different models have been proposed for granular materials such as sand (Liu et al., 2006, 2014) and gravel (Zhang et al., 2010; Saberi et al., 2016). Constitutive modeling of clay interfaces is still scarce (Stutz and Mašín, 2017).

However, through an adaptable new framework for the modeling of interfaces (Stutz et al., 2016; Stutz and Mašín, 2017), this gap has been closed for monotonic stress paths at interfaces. To extend this framework, the well-known intergranular strain concept (Niemunis and Herle, 1997) has been adapted to model interfaces. The intergranular strain concept is used in combination with a fine- and coarse-grained

ORCID: Hans Henning STUTZ, https://orcid.org/0000-0003-3360-1243

interface model as well as a reduced stress and strain tensor notation. This intergranular strain model was first used by Arnold (2008) to simulate cyclic loaded interfaces. The approach of Arnold (2008) is enhanced by assuming simple shear conditions at the interface.

After validating the new concept using experimental data for granular interfaces, the models are applied in some finite-element simulations to demonstrate the capabilities and benefits in computation. The results of a direct-shear interface test simulation are discussed below.

In addition to the cyclic modeling of interfaces, the influence of using more advanced interface models when dealing with sensitive marine clays is also shown. A toroidal penetrometer (Yan et al., 2011; Randolph et al., 2012; Stanier and White, 2015) has been modeled and the influences of different model combinations have been studied. The example is chosen to demonstrate that the influence and choice of interface model are also quite important in non-typical examples.

This paper concludes with a brief discussion of the results and gives an outlook for interface modeling, taking into consideration the special needs in offshore conditions.

2 Intergranular strain concept for interfaces

The intergranular strain concept was developed to prevent excessive ratcheting upon cyclic loading and to model the small strain behavior of soil continua (Niemunis and Herle, 1997). By introducing an additional state variable that represents the mircomechanic interlayer deformation between the different grains in the grain skeleton, the intergranular strain concept has been developed. This concept is used in many different constitutive applications to model the small-strain and cyclic behavior of soils (Henke and Grabe, 2008; Hong et al., 2017; Sheil and McCabe, 2017). In addition, the intergranular strain concept has been further improved and used to invent a new class of hybrid elasto-hypoplastic models (Fuentes and Triantafyllidis, 2015; Triantafyllidis, 2015).

The intergranular strain concept was adapted for the modeling of fine-grained soils by Mašín (2013). Herle and Nübel (1999) and Arnold and Herle (2006) developed the first hypoplastic interface model. Stutz et al. (2016, 2017) and Stutz and Mašín (2017) recently proposed different kinds of enhanced hypoplastic sand and new hypoplastic fine-grained interface models. These models have demonstrated a good capability to model monotonic stress and strain paths. However, these models are not able to capture the stiffness at small strains and cyclic stress paths. To improve and enrich these models, the extension of the intergranular strain concept (Niemunis and Herle, 1997) has been implemented into these models. Arnold (2008) implemented the first interface of the intergranular strain concept. The reduced strain and stress tensors (Arnold, 2008) are insufficient and will be replaced by the approach proposed by Stutz et al. (2016).

The intergranular model formulation of the hypoplastic models is expressed by

$$\dot{\boldsymbol{T}} = \boldsymbol{\mathcal{M}} : \boldsymbol{D}, \tag{1}$$

where $\boldsymbol{\mathcal{M}}$ is a fourth-order tangent stiffness material tensor, $\dot{\boldsymbol{T}}$ is the stress rate tensor, and $\dot{\boldsymbol{D}}$ is the strain rate tensor. This tangent stiffness material tensor is derived by interpolating between different states. The intergranular strain symmetric second-order tensor $\boldsymbol{\delta}$ is used. The intergranular layer deformation and the soil skeleton rearrangement are captured using $\boldsymbol{\delta}$. The normalized magnitude of the intergranular strain is expressed as

$$\rho = \frac{\|\boldsymbol{\delta}\|}{R}, \tag{2}$$

where R is the maximum constant value of the intergranular strain. The directional tensor for the intergranular strain is defined as

$$\hat{\boldsymbol{\delta}} = \begin{cases} \boldsymbol{\delta}/\|\boldsymbol{\delta}\|, & \text{if } \boldsymbol{\delta} \neq 0, \\ \boldsymbol{0}, & \text{if } \boldsymbol{\delta} = 0. \end{cases} \tag{3}$$

The stiffness $\boldsymbol{\mathcal{M}}$ is calculated using the fourth-order $\boldsymbol{\mathcal{L}}$ and the second-order constitutive tensor $\boldsymbol{N}$ by the following interpolation function:

$$\boldsymbol{\mathcal{M}} = [\rho^{\chi} m_{\mathrm{T}} + (1-\rho^{\chi}) m_{\mathrm{R}}] f_{\mathrm{s}} \boldsymbol{\mathcal{L}} + \begin{cases} \rho^{\chi}(1-m_{\mathrm{T}}) f_{\mathrm{s}} \boldsymbol{\mathcal{L}} : \hat{\boldsymbol{\delta}} \otimes \hat{\boldsymbol{\delta}} + \rho^{\chi} f_{\mathrm{s}} f_{\mathrm{d}} \boldsymbol{N} \hat{\boldsymbol{\delta}}, & \text{if } \hat{\boldsymbol{\delta}} : \boldsymbol{D} > 0, \\ \rho^{\chi}(m_{\mathrm{R}} - m_{\mathrm{T}}) f_{\mathrm{s}} \boldsymbol{\mathcal{L}} : \hat{\boldsymbol{\delta}} \otimes \hat{\boldsymbol{\delta}}, & \text{if } \hat{\boldsymbol{\delta}} : \boldsymbol{D} \leq 0, \end{cases} \tag{4}$$

where f_{s} and f_{d} are the barotropy and pyknotropy factors, χ controls the non-linearity of the stiffness on

the intergranular strain, m_T is the ratio of the shear modulus during 90° change of loading direction to the elastic shear modulus, and m_R is defined by the ratio of the maximum shear modulus to the elastic shear modulus. The evolution of $\dot{\boldsymbol{\delta}}$ is expressed as

$$\dot{\boldsymbol{\delta}} = \begin{cases} \left(\boldsymbol{\mathcal{I}} - \hat{\boldsymbol{\delta}} \otimes \hat{\boldsymbol{\delta}} \rho^{\beta_\mathrm{r}}\right) : \boldsymbol{D}, & \text{if } \hat{\boldsymbol{\delta}} : \boldsymbol{D} > 0, \\ \boldsymbol{D}, & \text{if } \hat{\boldsymbol{\delta}} : \boldsymbol{D} \leq 0, \end{cases} \tag{5}$$

where $\boldsymbol{\mathcal{I}}$ is the unity tensor, and β_r is a material parameter controlling the intergranular strain rate of decay.

Stutz et al. (2016) proposed using the following intergranular strain tensor at the interface:

$$\boldsymbol{\delta} = \begin{bmatrix} \boldsymbol{\delta}_{11} & \boldsymbol{\delta}_{12} & \boldsymbol{\delta}_{13} \\ \boldsymbol{\delta}_{21} & \boldsymbol{\delta}_{22} & \boldsymbol{\delta}_{23} \\ \boldsymbol{\delta}_{31} & \boldsymbol{\delta}_{32} & \boldsymbol{\delta}_{33} \end{bmatrix} = \begin{bmatrix} \boldsymbol{\delta}_\mathrm{n} & \boldsymbol{\delta}_x & \boldsymbol{\delta}_y \\ \boldsymbol{\delta}_x & \boldsymbol{\delta}_\mathrm{p} & 0 \\ \boldsymbol{\delta}_y & 0 & \boldsymbol{\delta}_\mathrm{p} \end{bmatrix}, \tag{6}$$

where $\boldsymbol{\delta}_x$ and $\boldsymbol{\delta}_y$ are the intergranular strain in the x and y directions, $\boldsymbol{\delta}_\mathrm{n}$ is the intergranular strain normal to the interface, and $\boldsymbol{\delta}_\mathrm{p}$ is the in-plane direction. When considering the modeling assumptions instead of using isotropic stress and strain conditions at the interface, the following Voigt notation is introduced for the reduced strain tensor:

$$\boldsymbol{\delta} = [\ \boldsymbol{\delta}_\mathrm{n}\ \ 0\ \ \boldsymbol{\delta}_x\ \ \boldsymbol{\delta}_y\ ]^\mathrm{T}. \tag{7}$$

Note that the in-plane intergranular strain is assumed to be $\boldsymbol{\delta}_\mathrm{p} = 0$. The intergranular strain tensor is thus considered an odeometric initial state instead of an isotropic state (Stutz et al., 2016). This is justified and proven by assuming a simple-shear condition at the interface (Stutz et al., 2016; Stutz and Mašín, 2017).

Arnold (2008) also remarked on the correct initialisation of the model after odeometric loading of the interface. The intergranular strain $\boldsymbol{\delta}_\mathrm{n} = 0$, $\boldsymbol{\delta}_x = R/\sqrt{3}$, and $\boldsymbol{\delta}_y = R/\sqrt{3}$ should be introduced under purely odeometric loading conditions. Mašín (2014) modified the intergranular strain concept for clays. The modified equations for m_R are

$$\begin{aligned} m_\mathrm{R} = {} & p_\mathrm{r} A_\mathrm{g} \left(\frac{p}{p_\mathrm{r}}\right)^{n_\mathrm{g}} \frac{4 A_\mathrm{m} \alpha_\mathrm{g}}{2 p \alpha_\mathrm{E}} \left(\frac{\lambda^* \kappa^*}{\lambda^* + \kappa^*}\right) \\ & \cdot \left(1 - \nu_\mathrm{pp} - 2\frac{\alpha_\mathrm{E}}{\alpha_\nu^2} \nu_\mathrm{pp}^2\right)^{-1}, \end{aligned} \tag{8}$$

$$m_\mathrm{T} = m_\mathrm{rat} m_\mathrm{R}, \tag{9}$$

where p_r is the reference stress of 1 kPa, A_g and n_g are the parameters describing the dependency to the shear modulus at very small strain, p is the mean stress, A_m is used as a algebraic manipulation for the model (Mašín, 2014), α_g and α_ν are anisotropy coefficients, α_E is the anisotropy ratio of Young's modulus, λ^* is a model parameter, κ^* is the parameter describing the volumetric unloading behaviour, ν_pp is the the direction dependent on Poisson's ratio, and m_rat is a parameter for the intergranular strain concept.

For this, the following parameters for the clay intergranular strain concept are used: A_g, n_g, β_r, and χ (Mašín, 2014).

More details about the different granular- and fine-grained hypoplastic model formulations are given in Appendices A and B. These models are extended by the intergranular strain concept described above.

3 Enhanced interface modeling

As described above, the modified stress, strain, and intergranular strain rate tensors as defined in Eq. (6) are used for this enriched modeling of the previous version of the interface intergranular strain model by Arnold (2008). In the following, the two different models are used to demonstrate the differences between the new and the old approaches by Arnold and Herle (2006) and Arnold (2008). The model of Arnold (2008) is abbreviated as AH and the new model of Stutz et al. (2016) as HvWE.

The AH model uses the reduced stress and strain conventions as follows: $\sigma_\mathrm{p} = \sigma_\mathrm{n}$, $\varepsilon_\mathrm{p} = \varepsilon_\mathrm{n}$, and $\boldsymbol{\delta}_\mathrm{p} = \boldsymbol{\delta}_\mathrm{n}$, where σ_p is the in-plane stress, σ_n is the normal stress, ε_p is the in-plane strain, and ε_n is the normal strain. The simulations are conducted using the parameters for sands (Table 1, where k is the sensitivity degradation, A is a parameter that controls the ratio between the volumetric and shear strain components, s_f and s_ini are the final and initial values for the soil sensitivity, and the other parameters are explained in the text and appendices).

The experimental data used are from cyclic constant-normal load tests conducted in a direct shear device modified by Uesugi et al. (1989) (Fig. 1). The soil was a Toyoura sand that was used on a rough structural steel surface. The one-way cyclic load path (Fig. 1) shows the differences between both reduced tensor notations. Neither the newer approach of Stutz et al. (2016) nor the approach

Table 1 Parameters for the hypoplastic model for Toyura sand (Arnold, 2008), Clay I (Mašín, 2014), and Clay II (Ragni et al., 2016)

Soil	Sand parameter								Interface	
	φ_c (°)	h_s (MPa)	n	e_{d0}	e_{c0}	e_{i0}	α	β	κ_r	d_s(mm)
Toyura	31	1000	0.29	0.61	0.96	1.09	0.13	2	0.98	3

Soil	Clay parameter										Interface	
	φ_c (°)	N	λ	κ	ν	α_g	k	A	s_f	s_{ini}	κ_r	d_s (mm)
Clay I	21.9	1.19	0.095	0.015	0.1	2	–	–	–	–	0.95	0.5
Clay II	34	0.114	0.013	1.697	0.1	–	0.05	0.2	1.0	2.9	0.95	0.75

Soil	Intergranular strain parameter							
	R	m_T	m_R	χ	β_r	A_g	m_{rat}	n_g
Toyura	1×10^{-10}	2.5	5	6	0.5	–	–	–
Clay I	5×10^{-5}	–	–	0.9	–	270	1	0.5

of Arnold (2008) fits the experimental data exactly. The HvWE model is able to capture the initial stiffness but shows a slower decrease with increasing cycles to the residual shear stress. The AH model shows a low peak strength in the first cycle and a lower residual mobilized shear strength. The next simulation is the two-way cyclic loading conducted by Uesugi et al. (1989). The shearing was applied in the test of Uesugi et al. (1989) with an amplitude of ±1 mm. As with the one-way cyclic simulation, the HvWE model captures the shear strength shear displacement behavior slightly better than the AH model (Figs. 2a and 2c). For the shear behavior, only small improvements between the AH and HvWE models are visible. Considering the normal strain-displacement behavior (Fig. 2b), it can be seen that the AH model has a more excessive accumulation of the normal strain, which is obviously due to the isotropic formulation of the AH model. Instead of the 1/3 for the oedometric conditions, the strain will be incorporated more excessively into the constitutive formulation.

After the comparison of differences between AH and HvWE for constant normal stiffness condition, it can be concluded that the volumetric response will be particularly important. The same can be observed using the clay interface models with and without the intergranular strain concept.

One major benefit of using continuum models as interface models is the possibility and flexibility of using the same parameters that are used within the soil itself. Therefore, only the standard model parametrisation must be done.

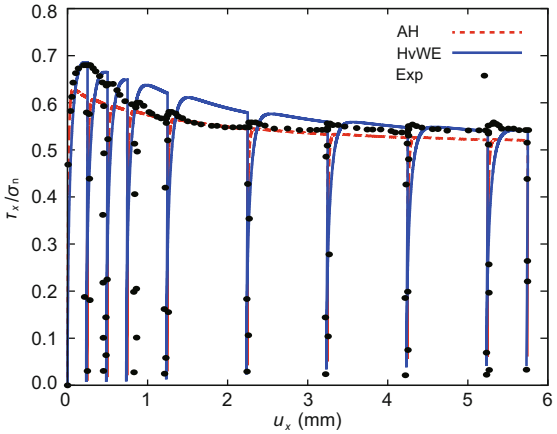

Fig. 1 Shear displacement u_x versus stress ratio T_x/σ_n for a fixed displacement rate ±0.05 mm using a σ_0 = 100 kPa (Exp indicates experimental data)

The only two additional parameters needed are the surface roughness coefficient κ_r and the shear zone thickness d_s. Based on Arnold and Herle (2006) and Stutz et al. (2016), the surface roughness coefficient is defined as the ratio between the critical state friction angle in the interface and the soil ($\kappa_r = \varphi_c^{int}/\varphi_c^{soil}$). This ratio can often be estimated.

The shear zone thickness itself is more difficult. Experimental research for granular soil-structure interfaces shows that the thickness of the interface zone can be varied between 3.5 to 15 times the mean grain size diameter d_{50}. In clays, the same assumption is often used.

Arnold (2008) proposed the following calibration concept for both parameters after adjusting the localization of the shear stress-strain/displacement response between simulation and experiments. This

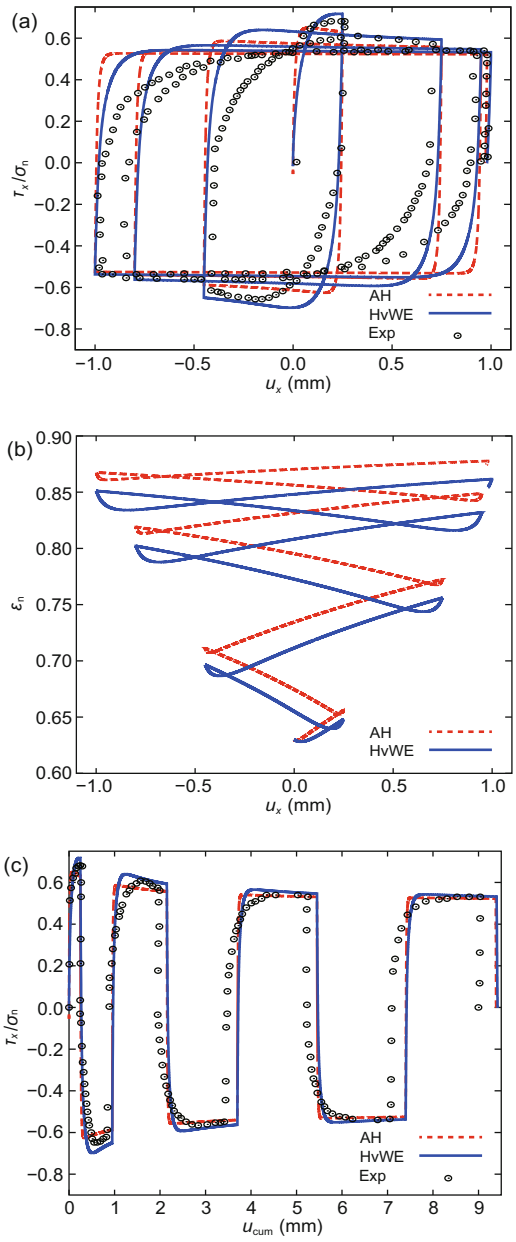

Fig. 2 Shear displacement versus stress ratio for a fixed displacement rate ± 0.05 mm using a $\sigma_0 = 100$ kPa: (a) stress ratio T_x/σ_n vs. shear displacement u_x; (b) vertical strain ε_n vs. shear displacement u_x; (c) stress ratio T_x/σ_n vs. accumulated displacement u_{cum}. Experimental data comes from Uesugi et al. (1989)

is done by calibrating d_s. In the second step with κ_r, the correct value of the asymptotic stress is adjusted.

4 Finite-element simulations

The section shows the use of the intergranular strain concept for interfaces in finite-element simulations using the hypoplastic soil and interface model. The general simulation purpose software Abaqus (Hibbit et al., 2015) is used and therefore also the implementation scheme of Stutz et al. (2017). This implementation uses a Fortran subroutine for frictional contacts (FRIC). In this scheme, a user-defined material model (UMAT) subroutine for the computation of the stress and strains is called. As proposed by Stutz et al. (2017), the general method can be used with any kind of continuum model (developed parallel to the idea of Weißenfels and Wriggers (2015)). In this method, the interface problem is formulated as a constitutive problem and not as an advanced numerical treatment. More details about the implementation can be found in (Stutz et al., 2017).

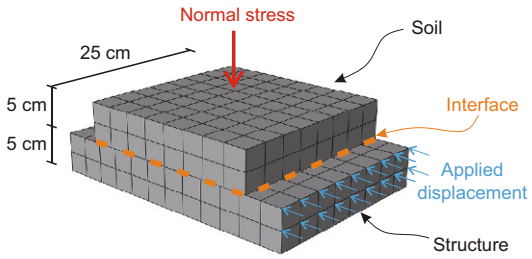

Fig. 3 Direct interface shear boundary value problem

The finite-element boundary value problem is the same as the one used by Stutz et al. (2017) (Fig. 3). The overlaying soil is sheared against a structural part. In both parts, the contact interface is defined. This model is used with 10 loading cycles. The deformation amplitude of ± 7.5 mm at the structural part is applied. The hypoplastic granular model of Stutz et al. (2016) and the clay model of Stutz et al. (2017) modified with the intergranular strain concept as described above are used as the interface models.

The parameters in this simulation (Table 1) are used for the interface and the soil in the bottom part of the model.

4.1 Simulation of cyclic interface tests

Three different simulations are calculated with a Gauss-point integration using an Euler-forward scheme (Fig. 4). All simulations are done for 10 cycles. Fig. 5 shows the stress-displacement graphs for the 1st, 5th, and 10th cycles. The shear stress contour computed in the finite element model is shown.

Comparison of the graphs from the full finite

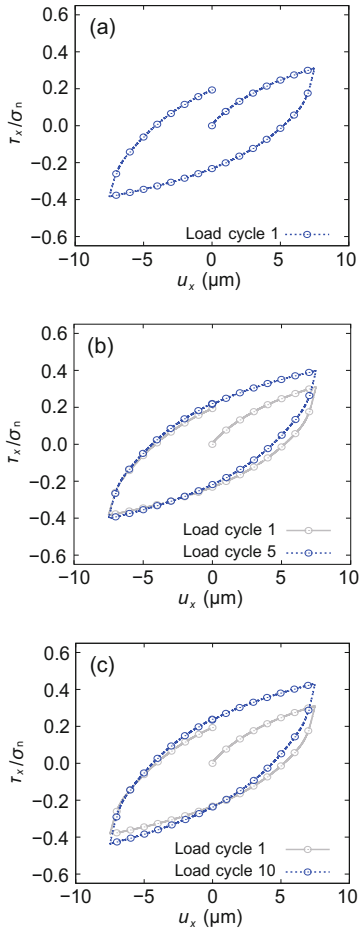

Fig. 4 Gauss-point integration using an Euler-forward scheme: (a) cycle 1; (b) cycle 5; (c) cycle 10

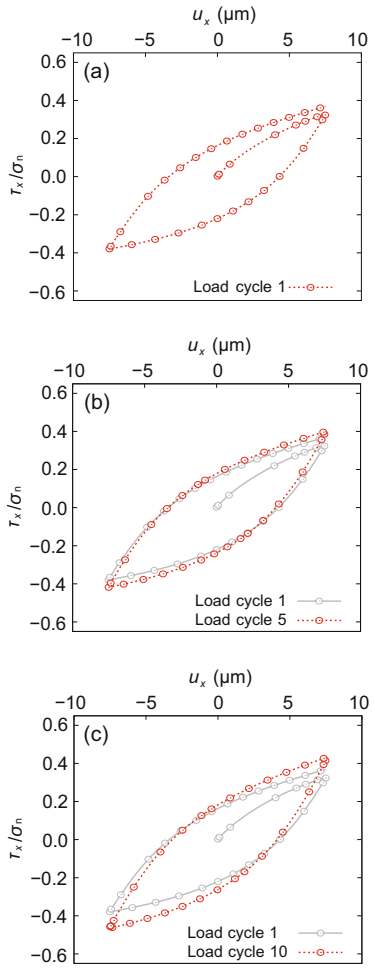

Fig. 5 Hypoplastic granular interface model: (a) cycle 1; (b) cycle 5; (c) cycle 10

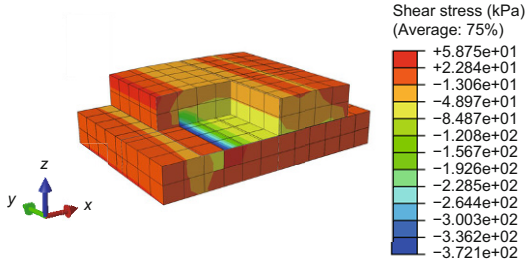

Fig. 6 Finite element simulations using the Mohr-Coulomb. Note: for interpretation of the references to color in the figure legend, the reader is referred to the web version of this article

element and Gauss-point algorithm shows good agreement between both solutions. However, small differences can be observed because the soil specimen in the overlaying soil deforms and the normal contact stresses change. Thus, the general global model response changes in the finite element simulation. The finite-element results using the Mohr-Coulomb contact (Fig. 6) are not able to simulate the 1.5 cycles because convergence is not achieved. Investigations of the deformed finite element model show that the strong localizations at the interface lead to convergence problems, whereas the hypoplastic interface model (Fig. 7) shows good simulation capabilities for 10 cycles. With an increasing cycle number, the sample shows a more pronounced stress localization. Similar trends are observed in experiments by De-Jong and Westgate (2009).

Figs. 8–10 shows the comparison of finite element simulations using the hypoplastic clay model in the soil and for the interface. Fig. 8 shows the use of the Mohr-Coulomb interface model. Table 1 gives the parameters for the clay interface simulations. The results indicate that when using a non-homogeneous modeling strategy (hypoplasticity with Mohr-Coulomb contact), the behavior is different when using a hypoplastic interface model with the same theoretical background. The use of the

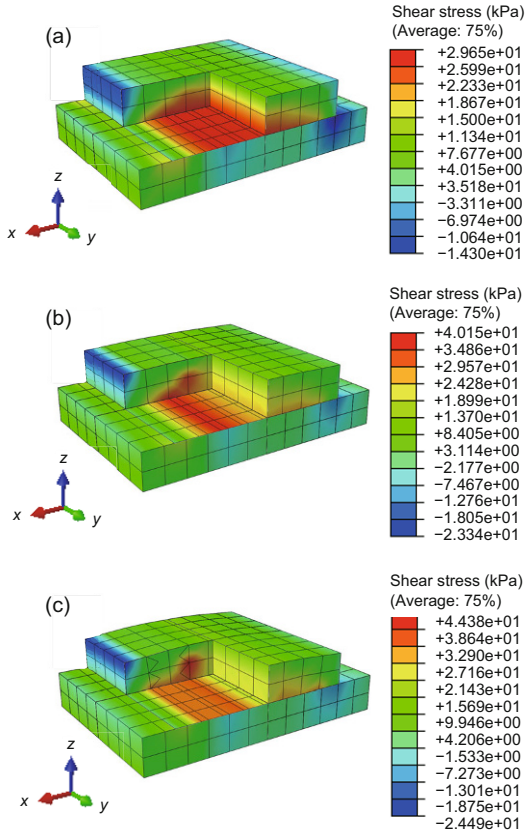

Fig. 7 Hypoplastic granular interface model: (a) cycle 1; (b) cycle 5; (c) cycle 10. Note: for interpretation of the references to color in the figure legend, the reader is referred to the web version of this article

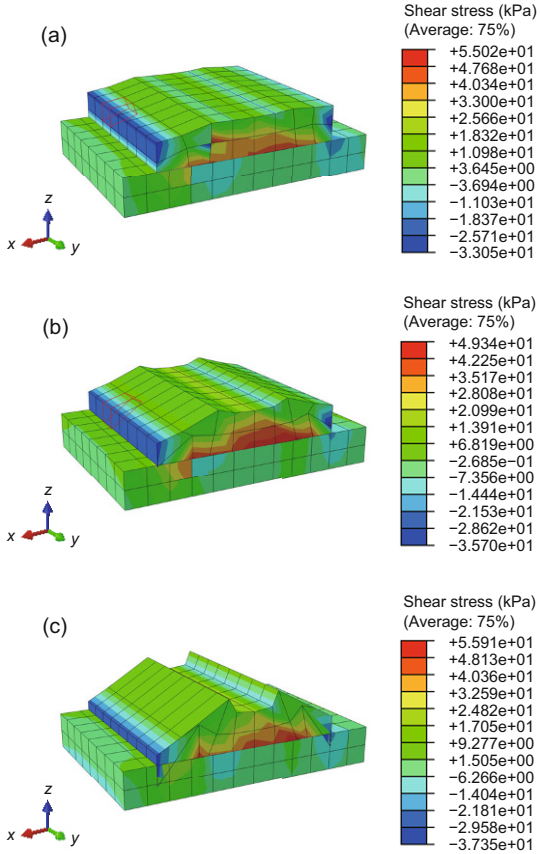

Fig. 8 Cyclic calculation using the Mohr-Coulomb: (a) cycle 1; (b) cycle 5; (c) cycle 10. Note: for interpretation of the references to color in the figure legend, the reader is referred to the web version of this article

Mohr-Coulomb model in particular leads to differences and convergence issues. One reason for this is the strong localization (Fig. 3). The major fact is that some elements at the interface are in slip, and neighboring elements are in the stick condition. The global finite element mesh convergence can therefore not be achieved.

In general, a model at soil-structure interfaces with smooth transition behavior is advantageous.

5 Simulations of the toriodal penetrometer for offshore site investigations

Development of a novel penetrometer for soil characterization is needed for the low effective stress conditions at the seabed surface. This is a highly demanding field (Stanier and White, 2015). Alongside different T-Bar and Ball penetrometers (Yan et al., 2011), the toroidoal penetrometer seems to be a suitable characterization method for the in-situ undrained shear strength profile. In addition to the use for the penetration characterization at such effective stress conditions, the axial pipeline sliding resistance for undrained or drained shearing taking into consideration consolidation phases can be measured by the torodial penetrometer. Because of the lack of field experience for the development of such a new type of penetrometer, finite-element analysis and modeling can increase the understanding of important design considerations. Furthermore, the modeling of such a torodial penetrometer is used to propose robust inverse analysis methods for converting the penetrometer resistance back to soil properties (Stanier and White, 2015). These methodical insights can be gained from the simulation using small and large deformation finite element analysis (Stanier and White, 2015).

Recent simulations (Stanier and White, 2015)

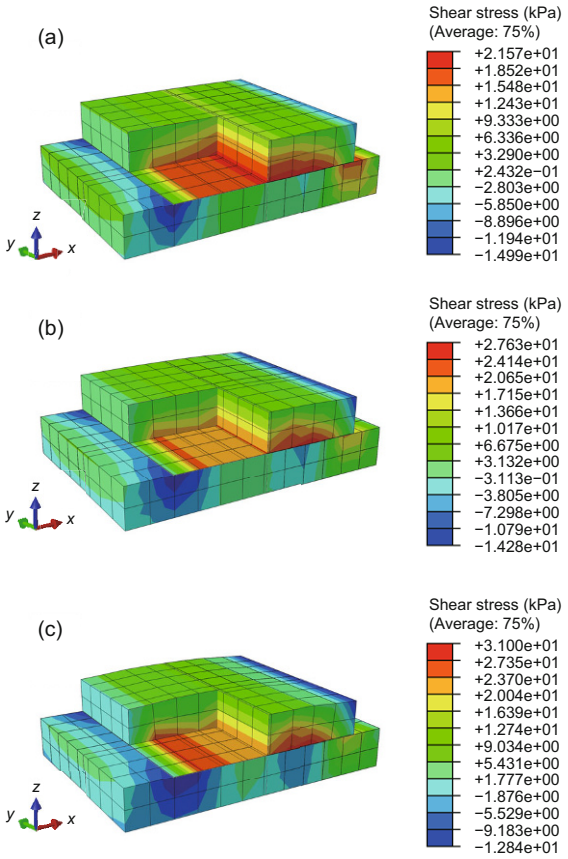

Fig. 9 Hypoplastic fine-grained interface model: (a) cycle 1; (b) cycle 5; (c) cycle 10. Note: for interpretation of the references to color in the figure legend, the reader is referred to the web version of this article

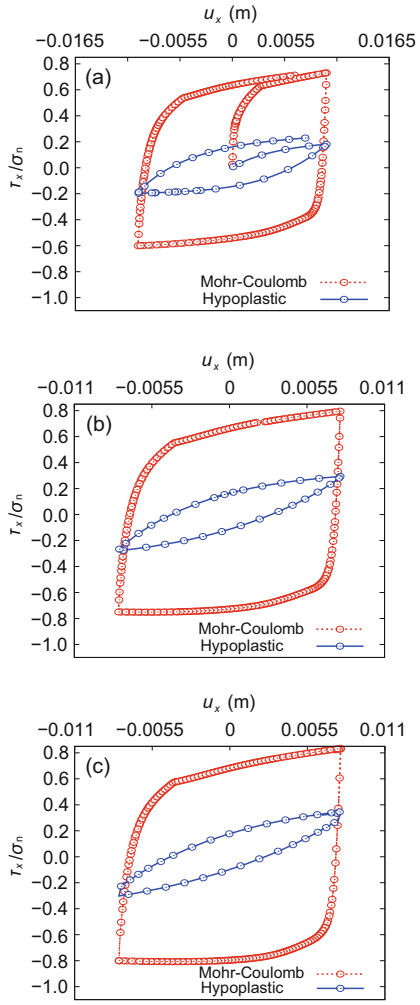

Fig. 10 Hypoplastic fine-grained interface model after cycle 1 (a), cycle 5 (b), and cycle 10 (c)

used a Tresca soil model, which does not capture the non-linear soil phenomena. Furthermore, the interface conditions in their simulations are captured using a simple Mohr-Coulomb frictional contact. However, these simplified interface models neglect important features and lead to uncertain assumptions for the stress-deformation pipeline-soil interface behavior. The results in this section can be found partly in (Stutz, 2016).

The aim of this section is to demonstrate the application and influence of a homogeneous modeling approach (hypoplastic soil and contact) compared with a simpler and inhomogeneous modeling approach (Mohr-Coulomb contacting with Tresca or hypoplastic soil model). It can also be shown that the contact model can have a significant role for offshore boundary value problems—even in non-classical examples (e.g. piles and suction bucket). The simulation is a simplified version of a pipeline penetration problem.

In particular, with respect to the inherent soil characteristics that do not exist in the simple model formulation, the simulations concerning the penetration resistance of the toriodal penetromenter will be improved.

5.1 Geometry and finite element model for the toriodial penetrometer

Yan et al. (2011) introduced the shallow torodial penetrometers. These are especially used for seabed characterization in pipeline geomechanics.

The idea is that the penetration resistance can be measured by pushing the torodial penetrometer to the seabed (Fig. 11, where T_1 is the applied torsional force). In addition, after deployment at a certain depth, the torodial penetrometer is shear against the soil. Through this application of a torsional load, the

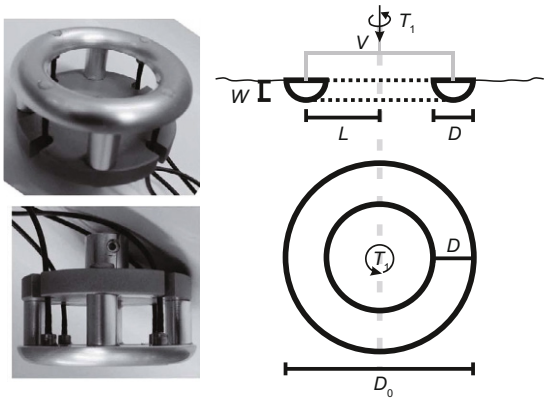

Fig. 11 Geometry of the the shallow penetrometer modified from Yan et al. (2011)

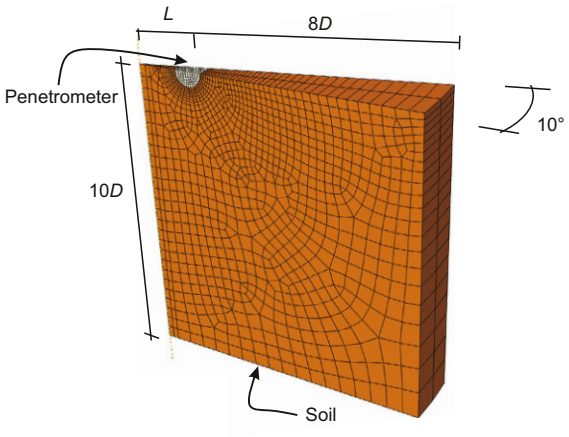

Fig. 12 Mesh and geometry of the boundary value problem for the shallow penetrometer considering cyclic symmetry (10° section; Stutz (2016))

axial pipeline shearing resistance can be determined. Because of the toroidal shape, it is possible to shear the interface against the soil up to nearly unlimited shear displacements and characterize the large deformation behavior. Furthermore, the effects of partial consolidation at the soil-pipeline interface as well as the effect of shearing rate can be tested.

This unique idea leads to an improvement of the measurement and in-situ characterization for pipeline design. Yan (2013) showed that this testing methodology is suitable for in-situ seabed characterization.

Yan (2013) compared different penetrometer sizes for a ball and a torodial penetrometer to find an optimal size for the toroidal penetrometer. The geometry of the toroidal penetrometer is described by the relationship between the length of the lever arm L and the diameter of the spherical ring D. Typical dimensions of such devices are $L = 200$ mm and $D_0 = 500$ mm (ratio $L/D = 2$). Fig. 11 gives the vertical load V and the embedment w. A geometry similar to that of the boundary value problem from Yan (2013) is used.

The boundary value problem uses the axial symmetry of the problem, considering the cyclic symmetry options from the finite element software.

Fig. 12 shows the mesh used in the boundary value problem. The mesh generation is done with eight node elements with linear interpolation functions. The penetrometer is modeled with a linear elastic constitutive model with a large stiffness (8-node elements). The soil-penetrometer interface is modeled with an augmented Lagrangian approach in the normal direction. The tangential interface behavior is modeled by the hypoplastic clay model proposed by Stutz and Mašín (2017) and Stutz et al. (2017).

At the lateral boundary the model boundaries are constrained against horizontal displacement and rotations (x- and y-directions). All degrees at the bottom are fixed. The circular boundaries are modeled by the cyclic symmetry option.

The soil around the penetrometer is modeled with the fine-grained soil hypoplastic model (Mašín, 2013), using the meta-stable extension to model the remoulding and softening of a silty carbonate offshore clay. Ragni et al. (2016) parametrized this soil and characterized this carbonate silty clay as a challenging soil. Detailed information about the hypoplastic model considering the meta-stable extension of the clay model can be found in Mašín (2007).

In addition to the hypoplastic model, Yan et al. (2011) used a Tresca soil model to compare the different models. Table 2 gives the Mohr-Coulomb and contact model parameters. ν_p is Poisson's ratio for a linear elastic model. μ_r and μ_s are the friction parameters for rough and smooth, respectively. For undrained modeling using the Mohr-Coulomb model, the frictional strength parameters ψ and φ are set to 0. Ragni et al. (2016) used an initial undrained shear strength s_u of 2.2 kPa. The same undrained shear strength is used in the following simulations.

Yan et al. (2011) neglected the unit weight because the effect of the unit weight is negligible. The penetrometer penetration is not modeled ('wish-in-place'). This simplification of the analysis is justified (Stanier and White, 2015) by comparable results

Table 2 Parameters for toroidal penetrometer and the Mohr-Coulomb, soil constitutive model

Penetrometer linear elastic parameters	E (kPa)	ν_p (-)
	10^{10}	0.25

Tresca soil model	E (kPa)	ν_p	s_u (kPa)	ψ (°)	φ (°)
	1103.4	0.495	2.2	0	0
Mohr-Coulomb contact	μ_s (-)	μ_r (-)	s_u (kPa)	ψ (°)	φ (°)
	0.05	0.95	–	–	–

from large displacement simulation results. In the simulations, only an axial displacement is applied.

5.2 Results of the penetrometer simulation

The different model combinations are compared and abbreviated as follows:

1. Tresca soil model/Mohr-Coulomb interface model (TR-MC);

2. Tresca soil model/hypoplastic fine-grained interface model (TR-HY);

3. Hypoplastic model (extension for sensitivity) /Mohr-Coulomb interface model (HY-MC);

4. Hypoplastic model (extension for sensitivity)/hypoplastic fine-grained interface model (HY-HY).

Assuming that after a normalized displacement of 0.1, the constant normalized force is reached.

Stanier and White (2015) considered the results as normalized displacement on the y-axis as u/D and on the x-axis with the normalized vertical load $V/s_u \cdot A_{con}$. Here, A_{con} is the contact area of the penetrometer and is calculated as

$$A_{con} = 2LD\pi. \tag{10}$$

Fig. 13a depicts the Tresca soil model. Six different simulations are conducted. Smooth ($\kappa_r = 0.05$) and fully rough ($\kappa_r = 1.0$) conditions are used with both interface models. In addition, limiting shear stress conditions of $\tau_{max} = s_u$ and $\tau_{max} = s_u/S$ with the Mohr-Coulomb interface model are used, where S is the soil sensitivity. Stanier and White (2015) used these limiting shear stress conditions because this will lead to a modeling of the remoulded state around the penetrometer.

Fig. 13 indicates the influences that must be considered when choosing a more sophisticated interface constitutive model. The Mohr-Coulomb friction model results in a higher load than the hypoplastic interface model.

Comparing the Tresca and hypoplastic soil model, it is obvious that the hypoplastic interface model is only advantageous when used with the latter. Nevertheless, all model combinations yield plausible results.

Using the hypoplastic soil model considering the effect of remoulding and softening, the model combination HY-MC results in higher normalized loads. The combinations using a hypoplastic soil and interface model result in lower normalized loads. The model combination HY-MC with the limiting shear stress (s_u/S) results in load-displacement close to the results using the HY-HY smooth simulation. However, using an HY-MC combination, the softening and remoulding behavior can not be modeled adequately.

This is proven by a comparison (Fig. 14). The model combinations (HY-MC/HY) with different maximal shear stresses as well as $\tau_{max} = s_u$ and $\tau_{max} = s_u/S$ conditions lead to improved model predictions compared with HY-MC combinations without limiting shear stress conditions.

The HY-HY simulations show a behavior that is similar to the HY-MC models using limited shear stress conditions (s_u, s_u/S).

6 Conclusions

As demonstrated above, the intergranular strain concept can be used for the modeling of interfaces. The difference is the use of the enhanced version of the reduced stress and strain rate tensors, which are used in Voigt notation considering the redefined mathematical operators (Stutz, 2016; Stutz et al., 2016). In addition, the modeling of cyclic and small-strain behavior of fine-grained interfaces is successfully shown.

For all these kinds of interfaces, the new extended intergranular strain concept-enhanced models have been successfully verified and validated. Considering such models will lead to the opportunity of modeling high-cyclic accumulation models using a concept like Niemunis et al. (2005).

Furthermore, the reduced stress and strain tensor concept can be used in conjunction with the numerical implementation scheme (Stutz et al., 2017). The benefit of using the concept of degradation of existing concepts for modeling the 3D soil continuum to interface models is the opportunity to easily

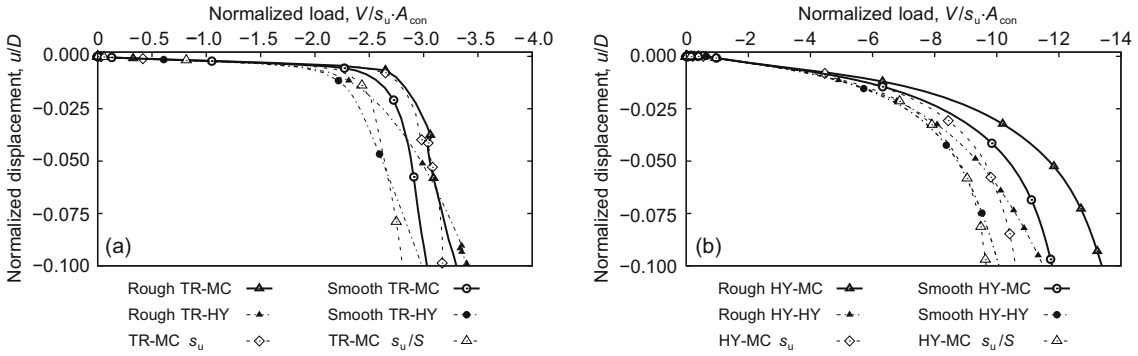

Fig. 13 Result for the different model simulations as normalized load-deformation results (Stutz, 2016): (a) simulations using the Tresca-continuum model; (b) simulations using the hypoplastic clay model with meta-stable structure extension

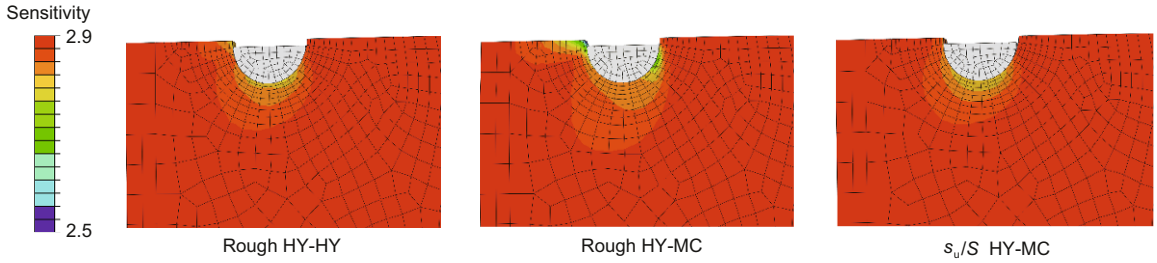

Fig. 14 Detail for the calculated sensitivity considering three different model simulations at a normalized displacement of $u/D = 0.1$. Note: for interpretation of the references to color in the figure legend, the reader is referred to the web version of this article

adapt constitutive models and the lack of specialized parameter calibration considering a fully calibrated constitutive model used to model the surrounding soil.

The modeling of the novel shallow penetrometer shows the importance of considering the accurate interface conditions. Instead of incorporation of assumptions, more advanced models can be used to implicitly consider the remoulding state and maximal limiting shear stress conditions. From Fig. 14, the behavior using the advanced models and the hypoplastic soil model with the simple Mohr-Coulomb model shows that it is not necessary to use shear stress assumptions at the interface if advanced interface models are used.

The use of such simpler models requires less calibration effort, but these models are limited. Because of the lack of experimental data, the more advanced models are hypothesized to give better predictions. Nevertheless, these more advanced models do not require any explicit assumption of the surrounding limiting shear stress as is the case for a remoulding state with the Mohr-Coulomb models.

This justifies the use of advanced models. In addition, the non-linear interface behavior will be considered and no artificial conditions will be introduced to the simulation. This is even the case in non-traditional interface modeling problems as can be seen from the penetrometer penetration simulation.

References

Arnold M, 2008. Application of the intergranular strain concept to the hypoplastic modelling of non-adhesive interfaces. The 12th International Conference of International Association for Computer Methods and Advances in Geomechanics (IACMAG), p.747-754.

Arnold M, Herle I, 2006. Hypoplastic description of the frictional behaviour of contacts. *In*: Schweiger HF (Ed.), Numerical Methods in Geotechnical Engineering. CRC Press, London, UK, p.101-106. https://doi.org/10.1201/9781439833766.ch14

DeJong JT, Westgate ZJ, 2009. Role of initial state, material properties, and confinement condition on local and global soil-structure interface behavior. *Journal of Geotechnical and Geoenvironmental Engineering*, 135(11):1646-1660. https://doi.org/10.1061/(ASCE)1090–0241(2009)135:11(1646)

DeJong JT, White DJ, Randolph MF, 2006. Microscale observation and modeling of soil-structure interface

behavior using particle image velocimetry. *Soils and Foundations*, 46(1):15-28. https://doi.org/10.3208/sandf.46.15

Fuentes W, Triantafyllidis T, 2015. ISA model: a constitutive model for soils with yield surface in the intergranular strain space. *International Journal for Numerical and Analytical Methods in Geomechanics*, 39(11):1235-1254. https://doi.org/10.1002/nag.2370

Gudehus G, 1996. A comprehensive constitutive equation for granular materials. *Soils and Foundations*, 36(1):1-12. https://doi.org/10.3208/sandf.36.1

Henke S, Grabe J, 2008. Numerical investigation of soil plugging inside open-ended piles with respect to the installation method. *Acta Geotechnica*, 3(3):215-223. https://doi.org/10.1007/s11440-008-0079-7

Herle I, Nübel K, 1999. Hypoplastic description of the interface behaviour. International Symposium on Numerical Models in Geomechanics, 7:53-58.

Hibbit D, Karlsson B, Sorensen P, 2015. Abaqus/Standard Analysis User's Manual. Hibbit, Karlsson, Sorensen Inc., Providence, USA.

Hong Y, He B, Wang LZ, et al., 2017. Cyclic lateral response and failure mechanisms of semi-rigid pile in soft clay: centrifuge tests and numerical modelling. *Canadian Geotechnical Journal*, 54(6):806-824. https://doi.org/10.1139/cgj-2016-0356

Liu HB, Song EX, Ling HI, 2006. Constitutive modeling of soil-structure interface through the concept of critical state soil mechanics. *Mechanics Research Communications*, 33(4):515-531. https://doi.org/10.1016/j.mechrescom.2006.01.002

Liu JM, Zou DG, Kong XJ, 2014. A three-dimensional state-dependent model of soil-structure interface for monotonic and cyclic loadings. *Computers and Geotechnics*, 61:166-177. https://doi.org/10.1016/j.compgeo.2014.05.012

Mašín D, 2007. A hypoplastic constitutive model for clays with meta-stable structure. *Canadian Geotechnical Journal*, 44(3):363-375. https://doi.org/10.1139/T06-109

Mašín D, 2013. Clay hypoplasticity with explicitly defined asymptotic states. *Acta Geotechnica*, 8(5):481-496. https://doi.org/10.1007/s11440-012-0199-y

Mašín D, 2014. Clay hypoplasticity model including stiffness anisotropy. *Géotechnique*, 64(3):232-238. https://doi.org/10.1680/geot.13.P.065

Mortara G, Mangiola A, Ghionna VN, 2007. Cyclic shear stress degradation and post-cyclic behaviour from sand-steel interface direct shear tests. *Canadian Geotechnical Journal*, 44(7):739-752. https://doi.org/10.1139/t07-019

Niemunis A, Herle I, 1997. Hypoplastic model for cohesionless soils with elastic strain range. *Mechanics of Cohesive-frictional Materials*, 2(4):279-299. https://doi.org/10.1002/(SICI)1099-1484(199710)2:4<279::AID-CFM29>3.0.CO;2-8

Niemunis A, Wichtmann T, Triantafyllidis T, 2005. A high-cycle accumulation model for sand. *Computers and Geotechnics*, 32(4):245-263. https://doi.org/10.1016/j.compgeo.2005.03.002

Pra-ai S, Boulon M, 2017. Soil-structure cyclic direct shear tests: a new interpretation of the direct shear experiment and its application to a series of cyclic tests. *Acta Geotechnica*, 12(1):107-127. https://doi.org/10.1007/s11440-016-0456-6

Ragni R, Wang D, Mašín D, et al., 2016. Numerical modelling of the effects of consolidation on jack-up spudcan penetration. *Computers and Geotechnics*, 78:25-37. https://doi.org/10.1016/j.compgeo.2016.05.002

Randolph MF, White JD, Yan Y, 2012. Modelling the axial soil resistance on deep-water pipelines. *Géotechnique*, 62(9):837-846. https://doi.org/10.1680/geot.12.OG.010

Saberi M, Annan CD, Konrad JM, et al., 2016. A critical state two-surface plasticity model for gravelly soil-structure interfaces under monotonic and cyclic loading. *Computers and Geotechnics*, 80:71-82. https://doi.org/10.1016/j.compgeo.2016.06.011

Sheil BB, McCabe BA, 2017. Biaxial loading of offshore monopiles: numerical modeling. *International Journal of Geomechanics*, 17(2):04016050. https://doi.org/10.1061/(asce)gm.1943-5622.0000709

Stanier SA, White DJ, 2015. Shallow penetrometer penetration resistance. *Journal of Geotechnical and Geoenvironmental Engineering*, 141(3):04014117. https://doi.org/10.1061/(asce)gt.1943–5606.0001257

Stutz H, 2016. Hypoplastic Models for Soil-structure Interfaces–Modelling and Implementation. PhD Thesis, Kiel University, Kiel, Germany.

Stutz H, Mašín D, 2017. Hypoplastic interface models for fine-grained soils. *International Journal for Numerical and Analytical Methods in Geomechanics*, 41(2):284-303. https://doi.org/10.1002/nag.2561

Stutz H, Mašín D, Wuttke F, 2016. Enhancement of a hypoplastic model for granular soil-structure interface behaviour. *Acta Geotechnica*, 11(6):1249-1261. https://doi.org/10.1007/s11440-016-0440-1

Stutz H, Mašín D, Sattari AS, et al., 2017. A general approach to model interfaces using existing soil constitutive models application to hypoplasticity. *Computers and Geotechnics*, 87:115-127. https://doi.org/10.1016/j.compgeo.2017.02.010

Triantafyllidis T, 2015. Holistic Simulation of Geotechnical Installation Processes: Numerical and Physical Modeling. Springer, Cham, Germany. https://doi.org/10.1007/978-3-319-18170-7

Uesugi M, Kishida H, Tsubakihara Y, 1989. Friction between sand and steel under repeated loading. *Soils and Foundations*, 29(3):127-137. https://doi.org/10.3208/sandf1972.29.3_127

Weißenfels C, Wriggers P, 2015. Methods to project plasticity models onto the contact surface applied to soil structure interactions. *Computers and Geotechnics*, 65:187-198. https://doi.org/10.1016/j.compgeo.2014.11.015

Yan Y, 2013. Novel Methods for Characterizing Pipe-soil Interaction Forces in situ in Deep Water. PhD Thesis, University of Western Australia, Perth, Australia.

Yan Y, White DJ, Randolph MF, 2011. Penetration resistance and stiffness factors for hemispherical and toroidal penetrometers in uniform clay. *International Journal of Geomechanics*, 11(4):263-275. https://doi.org/10.1061/(asce)gm.1943-5622.0000096

Zhang G, Wang LP, Zhang JM, 2010. Monotonic and cyclic modeling of interface between geotextile and gravelly soil. *International Journal for Numerical and Analytical Methods in Geomechanics*, 34(13):1346-1361. https://doi.org/10.1002/nag.865

Appendix A: Hypoplastic interface models

$$\dot{\boldsymbol{\sigma}} = \boldsymbol{\mathcal{L}} : \boldsymbol{D} + \boldsymbol{N} : \|\boldsymbol{D}\|, \tag{A1}$$

where $\boldsymbol{\mathcal{L}}$ and $\boldsymbol{N}$ are the fourth-order and second-order constitutive tensors, and $\dot{\boldsymbol{\sigma}}$ and $\boldsymbol{D}$ are the objective stress rate and stretching rate tensor, respectively. The hypoplastic model proposed by Gudehus (1996) included the pyknotropy that is the influence of the density and the barotropy for modeling the influence to the stress level. The proposed hypoplastic constitutive equation is expressed as

$$\dot{\boldsymbol{\sigma}} = f_{\mathrm{s}}(\boldsymbol{\mathcal{L}} : \boldsymbol{D} + f_{\mathrm{d}}\boldsymbol{N}\|\boldsymbol{D}\|), \tag{A2}$$

where f_{s} is the barotropy factor, and f_{d} is the pyknotropy factor. The fourth-order constitutive tensor $\boldsymbol{\mathcal{L}}$ is defined as

$$\boldsymbol{\mathcal{L}} = \frac{f_{\mathrm{s}}}{\hat{\boldsymbol{\sigma}} : \hat{\boldsymbol{\sigma}}}(F^2\boldsymbol{\mathcal{I}} + a^2\hat{\boldsymbol{\sigma}} \otimes \hat{\boldsymbol{\sigma}}), \tag{A3}$$

where a is the constitutive coefficient. The second-order constitutive tensor $\boldsymbol{N}$ is expressed as

$$\boldsymbol{N} = f_{\mathrm{s}}f_{\mathrm{d}}\frac{a \cdot F}{\hat{\boldsymbol{\sigma}} : \hat{\boldsymbol{\sigma}}}(\hat{\boldsymbol{\sigma}} + \hat{\boldsymbol{\sigma}}^*), \tag{A4}$$

where $\hat{\boldsymbol{\sigma}} = \boldsymbol{\sigma}/\mathrm{tr}(\boldsymbol{\sigma})$ and $\hat{\boldsymbol{\sigma}}^* = \hat{\boldsymbol{\sigma}} - \frac{1}{3}\mathbf{1}$ are deviator stresses. The Matsuoka-Nakai failure condition is defined as

$$F = \sqrt{\frac{\tan^2\psi}{8} + \frac{2 - \tan^2\psi}{2 + \sqrt{2}\tan\psi\cos(3\theta)}} - \frac{\tan\psi}{2\sqrt{2}}, \tag{A5}$$

where the Lode angle θ is expressed as

$$\cos(3\theta) = -\sqrt{6}\,\frac{\mathrm{tr}(\hat{\boldsymbol{\sigma}}^* \cdot \hat{\boldsymbol{\sigma}}^* \cdot \hat{\boldsymbol{\sigma}}^*)}{(\hat{\boldsymbol{\sigma}}^* : \hat{\boldsymbol{\sigma}}^*)^{3/2}}, \tag{A6}$$

with $\tan\psi = \sqrt{3}\,\|\hat{\boldsymbol{\sigma}}^*\|$. The barotropy factor f_{s} is defined as

$$f_{\mathrm{s}} = \frac{h_{\mathrm{s}}}{n}\left(\frac{e_{\mathrm{i}}}{e}\right)^{\beta}\frac{1 + e_{\mathrm{i}}}{e_{\mathrm{i}}}\left(\frac{-\mathrm{tr}(\boldsymbol{\sigma})}{h_{\mathrm{s}}}\right)^{1-n} \cdot \left[3 + a^2 - a\sqrt{3}\left(\frac{e_{\mathrm{i0}} - e_{\mathrm{d0}}}{e_{\mathrm{c0}} - e_{\mathrm{d0}}}\right)^{\alpha}\right]^{-1}, \tag{A7}$$

where h_{s}, β, α, and n are hypoplastic model parameters, e is the void ratio, and e_{c}, e_{d}, and e_{i} are limiting void ratios. The limiting values e_{d0}, e_{c0}, e_{i0} under mean zero pressure are implemented into the model as parameters.

$$\frac{e_{\mathrm{d}}}{e_{\mathrm{d0}}} = \frac{e_{\mathrm{c}}}{e_{\mathrm{c0}}} = \frac{e_{\mathrm{i}}}{e_{\mathrm{i0}}} = \exp\left(-\left(\frac{\mathrm{tr}(\boldsymbol{\sigma})}{h_{\mathrm{s}}}\right)^{n}\right). \tag{A8}$$

f_{d} (pyknotropy factor) is expressed as

$$f_{\mathrm{d}} = \left(\frac{e - e_{\mathrm{d}}}{e_{\mathrm{c}} - e_{\mathrm{d}}}\right)^{\alpha}. \tag{A9}$$

The constitutive coefficient a is defined as

$$a = \frac{\sqrt{3}\,(3 - \sin\varphi_{\mathrm{c}})}{2\sqrt{2}\sin\varphi_{\mathrm{c}}}, \tag{A10}$$

where φ_{c} is the critical state friction angle.

Appendix B: Fine-grained hypoplastic interface model

Mašín (2013) modified the general form of the hypoplastic constitutive formulation as

$$\dot{\boldsymbol{\sigma}} = f_{\mathrm{s}}\boldsymbol{\mathcal{L}} : \dot{\boldsymbol{\varepsilon}} - \frac{f_{\mathrm{d}}}{f_{\mathrm{d}}^{\mathrm{A}}}\boldsymbol{A} : \boldsymbol{d}\|\dot{\boldsymbol{\varepsilon}}\|, \tag{B1}$$

where $\dot{\boldsymbol{\varepsilon}}$ is the strain rate, $f_{\mathrm{d}}^{\mathrm{A}}$ describes the value of f_{d} at the asymptotic state boundary surface, and $\boldsymbol{d}$ is the asymptotic strain rate direction. $\boldsymbol{A}$ is defined as:

$$\boldsymbol{A} = f_{\mathrm{s}}\boldsymbol{\mathcal{L}} + \frac{\boldsymbol{\sigma}}{\lambda^*} \otimes \mathbf{1}. \tag{B2}$$

The $\boldsymbol{\mathcal{L}}$ tensor, representing the isotropic elasticity, is given by

$$\boldsymbol{\mathcal{L}} = \boldsymbol{\mathcal{I}} + \frac{\nu}{1 - 2\nu}\mathbf{1} \otimes \mathbf{1}, \tag{B3}$$

where ν controls the ratio between the bulk and the shear stiffnesses. The Hvorslev equivalent pressure p_{e}^* is given as

$$p_{\mathrm{e}}^* = p_{\mathrm{r}}\exp\left(\frac{N - \ln(1 + e)}{\lambda^*}\right), \tag{B4}$$

where N is a model parameter. The asymptotic strain rate direction $\boldsymbol{d}$ is assumed to be normal to the asymptotic state boundary surface. f_{d} is expressed by Mašín (2013) as

$$f_{\mathrm{d}} = \left(\frac{2p}{p_{\mathrm{e}}}\right)^{\alpha_{\mathrm{f}}}, \tag{B5}$$

where the exponent α_{f} controls the irreversible deformation inside the asymptotic state boundary surface (ASBS).

$$\alpha_{\mathrm{f}}=\ln\left(\frac{\lambda^*-\kappa^*}{\lambda^*+\kappa^*}\left(\frac{3+a_{\mathrm{f}}^2}{a_{\mathrm{f}}\sqrt{3}}\right)\right)/\ln 2, \tag{B6}$$

where a_{f} is defined as

$$a_{\mathrm{f}}=\frac{\sqrt{3}\,(3-\sin\varphi_{\mathrm{c}})}{2\sqrt{2}\sin\varphi_{\mathrm{c}}}. \tag{B7}$$

$f_{\mathrm{d}}^{\mathrm{A}}$ is defined as

$$f_{\mathrm{d}}^{\mathrm{A}}=2^{\alpha_{\mathrm{f}}}\left(1-F_{\mathrm{m}}\right)^{\alpha_{\mathrm{f}}/\omega}, \tag{B8}$$

where the exponent ω reads:

$$\omega=-\frac{\ln(\cos^2\varphi_{\mathrm{c}})}{\ln 2}+a_{\mathrm{f}}(F_{\mathrm{m}}-\sin^2\varphi_{\mathrm{c}}). \tag{B9}$$

The Matsuoka-Nakai factor F_{m} is expressed by

$$F_{\mathrm{m}}=\frac{9I_3+I_1I_2}{I_3+I_1I_2}. \tag{B10}$$

For the calculation of the Matsuoka-Nakai factor, the following invariants are used:

$$I_1=\mathrm{tr}(\boldsymbol{\sigma}),\ I_2=\frac{1}{2}\left(\boldsymbol{\sigma}:\boldsymbol{\sigma}-(I_1)^2\right),\ I_3=\det(\boldsymbol{\sigma}). \tag{B11}$$

The asymptotic strain rate direction $\boldsymbol{d}$ is given as

$$\boldsymbol{d}=\frac{\boldsymbol{d}^{\mathrm{A}}}{\|\boldsymbol{d}^{\mathrm{A}}\|}, \tag{B12}$$

where $\boldsymbol{d}^{\mathrm{A}}$ can be written as

$$\boldsymbol{d}^{\mathrm{A}}=-\hat{\boldsymbol{\sigma}}^*+\mathbf{1}\left(\frac{2}{3}-\frac{1}{4}F_{\mathrm{m}}^{1/4}\right)\frac{F_{\mathrm{m}}^{\xi/2}-\sin^{\xi}\varphi_{\mathrm{c}}}{1-\sin^{\xi}\varphi_{\mathrm{c}}}. \tag{B13}$$

The factor ξ controls the ratio of volumetric to shear strain. It is defined as

$$\xi=1.7+3.9\sin^2\varphi_{\mathrm{c}}. \tag{B14}$$

The model requires five parameters, φ_{c}, λ^*, κ^*, N, and ν.

中文概要

题　目：近海应用中土壤-结构界面的亚塑性模型

目　的：研究一种使用连续的土壤模型模拟土壤-结构界面的新方法，并阐述这些模型增强土壤-结构相互作用的建模方法。

创新点：1. 基于先前的亚塑性模型，通过将晶粒间应变的概念融入模型公式来模拟循环载荷。2. 整体性较好的模型具有更好、更精确的模拟结果。

方　法：1. 采用一种砂浆接触的力学方法，其中一个表面作为主面，另一个表面作为从属面。2. 采用砂浆接触的力学方法并结合用户定义的子程序，对土壤-结构界面进行建模。3. 基于先前的亚塑性模型，将晶粒间应变的概念融入模型公式来模拟循环载荷。

结　论：1. 整体性较好的模型具有更好、更精确的模拟结果。2. 本文提出的土壤-结构界面建模方法不仅提高了模拟结果，且在某些模拟中提高了数值收敛性。

关键词：亚塑性；接触面；循环荷载；细颗粒和粗粒土